Fall 1-31-1998

The In0.75Ga0.25As/In0.52Al0.48As/InP hall effect magnetic field sensor

Oleg Mitrofanov
New Jersey Institute of Technology

ABSTRACT

THE $In_{0.75}Ga_{0.25}As/In_{0.52}Al_{0.48}As/InP$ HALL EFFECT MAGNETIC FIELD SENSOR

by
Oleg Mitrofanov

The magnetic field sensor is produced from III-V group semiconductor materials. The structure is designed for molecular beam epitaxy growth technique (MBE) on the semiinsulating InP substrate. The sensitive element is the $In_{0.75}Ga_{0.25}As/In_{0.52}Al_{0.48}As$ heterostructure. The sensor uses the classic Hall effect in two-dimension electron gas (2DEG) formed at pseudomorphic strained epilayer of $In_{0.75}Ga_{0.25}As$. Properties of the 2DEG are preferential for the Hall effect sensor performance. Comparatively to bulk, electron mobility is higher. The device combines high magnetic field sensitivity and temperature stability. The sensor is designed for operation at room temperatures that makes it potentially useful in various practical applications.

THE $In_{0.75}Ga_{0.25}As/In_{0.52}Al_{0.48}As/InP$ HALL EFFECT SENSOR

by
Oleg Mitrofanov

A Thesis
Submitted to the Faculty of
New Jersey Institute of Technology
in Partial Fulfillment of the Requirements for the Degree of
Master of Science in Materials Science and Engineering

Interdisciplinary Program in Materials Science and Engineering

January 1998

APPROVAL PAGE

THE $In_{0.75}Ga_{0.25}As/In_{0.52}Al_{0.48}As/InP$ HALL EFFECT SENSOR

Oleg Mitrofanov

Dr. Roland A. Levy, Thesis Advisor — Date
Distinguished Professor of Physics, NJIT

Dr. John F. Federici, Committee Member, — Date
Professor of Physics, NJIT

Dr. Trevor A. Tyson, Committee Member, — Date
Professor of Physics, NJIT

BIOGRAPHICAL SKETCH

Author: Oleg Mitrfanov

Degree: Master of Science in Materials Science and Engineering

Date: January, 1998

Undergraduate and Graduate Education:

Master of Science in Materials Science and Engineering,
New Jersey Institute of Technology,
Newark, New Jersey, 1998

Bachelor of Physics,
Moscow State University,
Moscow, Russia, 1996

Major: Materials Science and Engineering

This thesis is dedicated to
my parents

ACKNOWLEDGMENT

The author expresses his gratitude to his advisor, Professor Roland A. Levy for his guidance, support, and inspiration during this research.

Special thanks to Professor John F. Federici and Professor Trevor A. Tyson for participating in the thesis committee.

The author appreciate help and suggestions from the CVD laboratory members, including: Vitaliy Sigal, Krit Aryusook, and Romanuja Narahari.

TABLE OF CONTENTS

TABLE OF CONTENTS
(Continued)

Chapter **Page**

LIST OF FIGURES

LIST OF TABLES

Table **Page**

CHAPTER 1

INTRODUCTION

1.1. Objective

A magnetic sensor is a transducer that converts a magnetic field into an electrical signal. Semiconductor magnetic sensors exploit galvanomagnetic effects due to the Lorentz force on charge carriers in semiconductors. The most often used of these effects is the Hall effect, which produces an electric field perpendicular to the magnetic induction vector and the original carrier deflection. Other galvanomagnetic effects include the magnetoresistance and the magnetoconcentration effect.

Semiconductor sensors occupy the leading position in the field of magnetic sensors. Magnetic devices made of semiconductors are used for direct magnetometers, as well as for displacement sensors of brushless motors in a videotape recorder and disk driver, contactless switches, and bill detectors in vending machines. The advantage of the Hall effect is that its intensity is linear within the range of magnetic field 10^{-8} T $< B <$ 1 T. This fact makes hall sensors applicable in various practical measurements of magnetic field. Here are some examples of magnetic induction within that range:

i) geomagnetic field	30-60 μT
ii) magnetic storage media	about 1 mT
iii) permanent magnets in switches	5-100 mT
iv) conductor carrying a 10 A current	1 mT

v) magnetic fields of bioobjects $< 1\ \mu T$

The performance of most planar silicon sensors declines in applications where nanotesta resolution is required. A principal factor that limits silicon hall sensors sensitivity is a low electron mobility. Up to present time the most sensitive instruments for measuring magnetic fields are superconductive quantum interference devices (SQUID). They successfully work at nanotesla range. However SQUIDs are not perfect since operation conditions require the temperature to be very low.

Advanced III-V semiconductor technologies are beginning to make their impact on magnetic sensors. Advantages of this family of semiconductors are the high electron mobility comparatively to silicon and a freedom in structure engineering. By means of molecular beam epitaxy (MBE), Hall devices have been fabricated which use the two-dimensional electron gas (2DEG) confined to a very thin (about 100 A) layer in a heterojunction structure as the active sensor layer. Described here is a highly sensitive magnetic sensor for room temperature applications. The semiconductor device uses the Hall effect in a quantum-well pseudomorphic InAlAs/InGaAs heterostructure. The sensor achieves a large sensitivity at room temperatures due to a high electron mobility and a low electron concentration in the active layer. It is expected that the quantum-well Hall device with low dimensional heterostructure has nanotesla resolution with a high signal-to-noise ratio.

The properties of the electron system in pseudomorphic heterostructures with quantum wells are different from those in the bulk. Design and fabrication of the sensors requires

the complete knowledge of involved processes, optimal operating conditions, and principal limits.

The objective of this work is to present our studies of semiconductor magnetic sensors, based on the Hall effect in the quantum-well InAlAs/InGaAs heterostructure

1.2. Literature Review

Up to present time most of the efforts had been devoted to silicon based Hall sensors. However this material is not perfect for magnetic sensors because of rather low mobility. It was also reported that Si devices manifest a high thermal drift comparatively to III-V based devices using 2DEG as an active layer (24).

2DEG heterostructures had been developed during the industrial production of field effect transistors in the $Ga_{1-x}Al_xAs/GaAs$, $Ga_{1-x}Al_xAs/Ga_{1-y}In_yAs/GaAs$, and $In_{1-x}Al_xAs/Ga_{1-y}In_yAs/InP$ systems. The use of a pseudomorphic strained GaInAs layer as the 2DEG channel has been demonstrated to be the best, because of its efficient charge transfer and confinement of the electrons in the channel due to the conduction band offset (1,2). Moreover, owing to the composition effect the decrease of the electron effective mass leads to a higher mobility (3).

Recently the Hall sensors in the InGaAs/InP material system have been reported (3). The element consisted of MBE grown pseudomorphic $In_{0.8}Al_{0.2}As/Al_{0.52}In_{0.48}As/InP$ heterostructures which were used for high electron mobility transistors. High room temperature mobilities of 16000 cm^2/Vs and sensitivities of 320 V/AT were obtained. A

very low temperature coefficient of the sensitivity of 0.035% K^{-1} was measured. A signal-to-noise ratio corresponding to a resolution of 60 nT were expected.

A high performance $In_{0.75}Ga_{0.25}As/Al_{0.52}In_{0.48}As/InP$ Hall sensor grown by MBE was reported in (4). The sensor manifested a high magnetic sensitivity (580 V A^{-1} T^{-1}) at room temperatures, fine resolution (350 nT), and low temperature coefficient (0.05% K^{-1}). The Hall sensor using properties of 2DEG in $In_{0.15}Ga_{0.85}As/Al_{0.3}Ga_{0.7}As/GaAs$ was discussed in (5). High bias current related sensitivity of 1000 V A^{-1} T^{-1} was achieved for single heterostructure GaAs/AlGaAs element (6). A poor temperature coefficient of the sensitivity of 0.7% K^{-1} was measured, which was attributed to the trap centers commonly found in GaAs/AlGaAs heterostructures. This drawback was overcome in GaAs/AlAs sensors with superlattice structure (7). They showed high sensitivities of 1200 V A^{-1} T^{-1} with moderate temperature coefficients of 0.1% K^{-1}.

Various aspects of 2DEG systems in heterostructures such as energy band structure, electron mobility, temperature affects were discussed in (8-10).

1.3. Background Information

2DEG hall sensors likewise most other magnetic sensors exploit the Lorentz force $\boldsymbol{F}$ on moving electrons in a semiconductor, metal, or an insulator,

$$\boldsymbol{F} = -q\boldsymbol{v}_n \times \boldsymbol{B}, \tag{1}$$

where q denotes the absolute value of the electron charge, $\boldsymbol{v}_n$ the electron velocity vector, and $\boldsymbol{B}$ the magnetic induction vector. An electron moves along a helix in a uniform magnetic field under the Lorentz force, and the helix axis is collinear with the direction of

the magnetic induction vector $\boldsymbol{B}$. In a uniform electric field an electron experience the Colomb force and moves along field lines in the direction opposite to the direction of the electric field vector $\boldsymbol{E}$. The total force that acts on an electron in electromagnetic field can be written in the form

$$\boldsymbol{F}=-q\boldsymbol{E}-q\boldsymbol{v}\times\boldsymbol{B}, \tag{2}$$

where $\boldsymbol{E}$ denotes the electric field vector. An average velocity of motion of a charge in crossed electric and magnetic fields is called the electrical drift velocity. Its direction is perpendicular to both fields and is dependent of the sign of the charge. The magnetic induction vector $\boldsymbol{B}$, that acts on the mobile carriers, relates to the magnetic field vector $\boldsymbol{H}$

$$\boldsymbol{B}=\mu_0\mu\boldsymbol{H}, \tag{3}$$

where μ_0 denotes the permeability of free space and μ the relative permeability of the sensor material.

Due to the Maxwell distribution, the carrier velocity is not uniform (11). Neglecting the statistical distribution of the electron velocity, the average drift-diffusion electron velocity v_n may be assumed. At low electric field the drift velocity v_n is proportional to the electric field strength $\boldsymbol{E}$ and the proportionality constant is defined as the mobility μ_n,

$$v_n=\mu_n\boldsymbol{E}. \tag{4}$$

For nonpolar semiconductors such as Ge and Si there are two scattering mechanisms which significantly affect the mobility, acoustic phonons and ionized impurities (12). The mobility decreases with temperature due to scattering on acoustic phonons

$$\mu_a \sim (m^*)^{-5/2} T^{3/2}, \tag{5}$$

where m^* denotes the conductivity effective mass (12, 13). Ionized impurity scattering mechanism manifests opposite temperature dependence. At low temperatures electron scattering on charged centers is the dominant process. With a temperature increase electrons obtain more energy and scatter on ionized impurities with less efficiency. As a result the mobility due to ionized impurities increases with temperature

$$\mu_i \sim (m^*)^{-1/2} T^{3/2} N_i^{-1} , \tag{6}$$

where N_i is the ionized impurity density. At room temperature most impurities are ionized and in general this scattering process must be taken into consideration.

The combined mobility which consists of the above two mechanisms is

$$\mu_n = (1/\mu_a + 1/\mu_i)^{-1}. \tag{7}$$

For polar semiconductors such as GaAs there is another important scattering mechanism, optical phonon scattering (13). The temperature dependence of the combined mobility can be approximated by expression

$$\mu_n \sim (m^*)^{-3/2} T^{3/2} . \tag{8}$$

The expression (8) also implies that as the effective mass increases, μ_n decreases.

The total electron current density $\boldsymbol{J}_n$ for zero magnetic induction ($\boldsymbol{B}$=0) is the sum of drift and diffusion components

$$\boldsymbol{J}_n(0) = qn\boldsymbol{v}_n = \sigma_n \boldsymbol{E} + qD_n \nabla n, \tag{9}$$

where the diffusion component is described by the diffusion coefficient D_n, which relates to the mobility through the Einstein equation (13)

$$D_n = \mu_n kT/q . \tag{10}$$

The conductivity σ_n is defined as the proportionality constant between current density vector and electric field vector and relates to the mobility as

$$\sigma_n = q\mu_n n \,. \tag{11}$$

When the magnetic field is applied the current density $\boldsymbol{J_n(B)}$ can be composed

$$\boldsymbol{J_n(B)} = \boldsymbol{J_n}(0) - \mu_n \boldsymbol{J_n(B)} \times \boldsymbol{B}. \tag{12}$$

Solving Eq. 12 with respect to $\boldsymbol{J_n(B)}$ leads to

$$\boldsymbol{J_n(B)} = [\boldsymbol{J_n}(0) - \mu_n \boldsymbol{B} \times \boldsymbol{J_n}(0) + (\mu_n)^2 \boldsymbol{B} \cdot \boldsymbol{J_n}(0)\boldsymbol{B}][1 + (\mu_n \boldsymbol{B})^2]^{-1}. \tag{13}$$

For nondegenerate semiconductors, however, the velocity distribution of the electrons and, hence, the velocity dependence of scattering mechanism, cannot be neglected (12). This effect can be described in terms of the scattering factor r_n for electrons,

$$r_n = \langle\tau^2\rangle / \langle\tau\rangle^2, \tag{14}$$

where τ denotes the relaxation time or mean free transit time between two successive electron collisions, which depends on the electron energy, and the brackets $\langle\rangle$ denote the average over the electron energy distribution. For semiconductors with spherical constant-energy surfaces $\tau \sim E^{-1/2}$ for phonon scattering, $\tau \sim E^{3/2}$ for ionized impurity scattering, and in general, $\tau \sim aE^{s}$ where a and s are constants. From Boltzmann's distribution for nondegenerate semiconductors the average value of the m-th power of τ is:

$$\langle \tau^{m} \rangle = \frac{\int_0^\infty \tau^{m} E^{3/2} \exp(-E/kT) dE}{\int_0^\infty E^{3/2} \exp(-E/kT) dE}. \tag{15}$$

The theoretical values r_n=1.18 for phonon scattering and r_n=1.93 for ionized impurity scattering (12). To the first order in $\boldsymbol{B}$, the electron velocity-dependent scattering can be accounted for by replacing the drift mobility μ_n by the Hall mobility

$$\mu_n^* = r_n \mu_n. \tag{16}$$

Submitting the Eq. (16) in the expression for the current density Eq. (14) results

$$\boldsymbol{J}_n(\boldsymbol{B})=[\boldsymbol{J}_n(0)- \mu_n^* \boldsymbol{B}\times\boldsymbol{J}_n(0)+\boldsymbol{K}(\mu_n^*)^2\boldsymbol{B}\cdot\boldsymbol{J}_n(0)\boldsymbol{B}][1+(\mu_n^*\boldsymbol{B})^2]^{-1}. \tag{17}$$

This equation describes the electron current density in an isotropic nondegenerate n-type semiconductor exposed to the magnetic induction $\boldsymbol{B}$ (11). The factor $\boldsymbol{K}$ summarizes effects of higher power of velosity distribution averages such as $<\tau^3>$. The equation describes galvanomagnetic effects at a constant temperature. But thermal effects are included through the temperature dependence of carrier concentration, mobility, and diffusion coefficient.

If carrier concentration gradients ∇n are negligible, as in a semiconductor slab with ohmic contacts the expression (9) reduces to

$$\boldsymbol{J}_n(0)=\sigma_n\boldsymbol{E}, \tag{18}$$

and the expression for current density simplifies to the form

$$\boldsymbol{J}_n(\boldsymbol{B})= \sigma_{nB}[\boldsymbol{E}+ \mu_n^*\boldsymbol{B}\times\boldsymbol{E}+\boldsymbol{K}(\mu_n^*)^2(\boldsymbol{B}\cdot\boldsymbol{E})\boldsymbol{B}], \tag{19}$$

with the magnetic-field dependent conductivity

$$\sigma_{nB}=\sigma_n[1+(\mu_n^*\boldsymbol{B})^2]^{-1}. \tag{20}$$

From the expression (19) it is clear that the current density substantially depends on the relative orientation of the vectors $\boldsymbol{E}$ and $\boldsymbol{B}$. If B is parallel to E and thus the vector

product is equal to zero ($\boldsymbol{B}\times\boldsymbol{E}=0$), then the current density $J_n(\boldsymbol{B})$ is parallel to the electric field vector $\boldsymbol{E}$ and equals to

$$J_n(\boldsymbol{B})=\sigma_{nB}[1+\boldsymbol{K}(\mu_n^{*}\boldsymbol{B})^2]\boldsymbol{E}, \tag{21}$$

The effect of the magnetic field induction dependence of the ratio $J_n(\boldsymbol{B})/\boldsymbol{E}$ is known as the magnetoresistance effect (11).

If the magnetic induction vector $\boldsymbol{B}$ is perpendicular to the electric field $\boldsymbol{E}$, the scalar product of $\boldsymbol{B}$ and $\boldsymbol{E}$ in the expression (19) equals to zero, and, hence, the electron current density can be written

$$J_n(\boldsymbol{B})=\sigma_{nB}(\boldsymbol{E}+\mu_n^{*}(\boldsymbol{B}\times\boldsymbol{E})). \tag{22}$$

This equation describes transverse galvanomagnetic effects for electrons in the case of negligible diffusion (11). The term $\mu_n^{*}(\boldsymbol{B}\times\boldsymbol{E})=-(\boldsymbol{v}\times\boldsymbol{B})$ is often interpreted as a transverse electric field counterbalancing the deflection of the carrier path under the Lorentz force.

A specific geometric configuration where the vectors $\boldsymbol{E}$ and $J_n(\boldsymbol{B})$ are in the x-y plane ($\boldsymbol{E}=(E_x, E_y, 0)$, $J_n(\boldsymbol{B})=(J_{nx}, J_{ny}, 0)$) and the magnetic induction vector $\boldsymbol{B}$ is parallel to the z direction ($\boldsymbol{B}=(0, 0, B)$) is essential for further discussion. The equation (22) breaks into a system of vector components equations

$$\begin{aligned} J_{nx}(B)&=\sigma_{nB}(E_x-\mu_n^{*}BE_y),\\ J_{ny}(B)&=\sigma_{nB}(E_y+\mu_n^{*}BE_x),\\ J_{nz}(B)&=0. \end{aligned} \tag{23}$$

The two limiting cases of the ratio J_{nx} and J_{ny} are of considerable interest. For $J_{nx} >> J_{ny}$ the y-direction component of current density can be assumed to be equal to zero, then the current density has only an x-component. Physically this assumption corresponds to the

hypothesis that when equilibrium is reached deflected electrons produce an electric field that, acting on other electrons, counterbalance the Lorentz force. The field is called the Hall field

$$E_H=Ey=-\mu_n^* BE_x=R_H J_{nx} B, \tag{24}$$

where

$$R_H=-\mu_n^*/\sigma_n=-r_n/qn \tag{25}$$

denotes the Hall coefficient. R_H is a material parameter which characterizes the magnitude of the Hall effect. The value of R_H depends on doping of the semiconductor material and on the temperature since the electron concentration is temperature dependent (13)

$$n(T)=\frac{1}{4}\left(\frac{2m^* k_B T}{\pi\hbar^2}\right)^{3/2}\exp\left[\frac{-(E_C-E_F)}{k_B T}\right], \tag{26}$$

here k_B denotes the Boltzman constant, and E_C , E_F the energies of conductive band and Fermi level respectively.

So far only electrons as current carriers were taken in consideration. This approach can be applied to a semiconductor material with electron conductivity. Holes, positive charge carriers, move in an electric field in the direction opposite to that of electron drift and similarly experience the Lorentz force

$$\boldsymbol{F}= q\boldsymbol{v}_p \times \boldsymbol{B}, \tag{26}$$

where $\boldsymbol{v}_p$ denotes the hole velocity vector. For a given $\boldsymbol{E}$ and $\boldsymbol{B}$ orientation both holes and electrons are deflected in the same direction. The Hall field for holes is

$$E_{Hp}=\mu_n^* BE_x, \tag{27}$$

Because the hole velocity vector is oriented opposite to the current density vector the sign of right hand term of equation is changed comparatively to the expression for electrons. The cartesian components of the current density $\boldsymbol{J}_p(\boldsymbol{B})$ are

$$\begin{aligned} J_{px}(B) &= \sigma_{pB}(E_x+\mu_n^* BE_y), \\ J_{py}(B) &= \sigma_{pB}(E_y-\mu_n^* BE_x), \\ J_{pz}(B) &= 0. \end{aligned} \tag{28}$$

Deflected electrons and holes produce the Hall fields that compensate each another. The Hall coefficient R_H depends on the sign of the charge and is negative for electrons and positive for holes.

The presence of the Hall field results in a rotation of the equipotential lines by the Hall angle θ_H with

$$\tan\theta_H = E_y/E_x = = -\mu_n^* B = \sigma_n R_H B. \tag{29}$$

The $J_{ny} << J_{nx}$ approach can be successfully applied in calculation of the Hall voltage in long sample. Consider an n-type semiconductor rectangular plate of thickness d, and a length L much larger then its width ($L >> W$). A voltage V_x applied along the plate generates the electric field

$$E_x = V_x/L, \tag{30}$$

in the plate. A magnetic field vector $\boldsymbol{B}$ oriented along z-axis deflects moving electrons and a voltage across width of the plate is generated.

Across a long, thin plate of thickness d carrying a current I, the Hall field produces the corresponding Hall voltage

$$V_H = WE_{Hn} = -W\mu_n^* BE_x = -W\mu_n^* BV_x/L. \tag{31}$$

Using the expression (25) for the Hall coefficient and the relation between current and current density the Hall voltage can be written

$$V_H=R_H I_x B/d, \tag{32}$$

where I_x denotes the current along x-axis.

The other limiting case (E_y=0) approximates conditions of a short-circuited Hall field or a wide short plate. A transverse current density components J_{ny} is not equal to zero and results in a rotation of the current lines described by the ratio

$$-J_{ny}/J_{nx}= \mu_n^* B=\tan\theta_l. \tag{33}$$

An important feature of the hall effect in the case of mixed conductivity is the fact that electrons and holes are deflected by the Lorentz force in the same direction because of opposite drift velocity and opposite sings of their electric charges. Expressions for the hall mobility and the Hall coefficient in the presence of two types of carriers can be presented in the form (12):

$$\mu_H = \frac{r_{H1} q_1 n_1 \mu_1^2 + r_{H2} q_2 n_2 \mu_2^2}{q_1 n_1 \mu_1 + q_2 n_2 \mu_2}; \tag{34}$$

$$R_H = \frac{r_{H1} q_1 n_1 \mu_1^2 + r_{H2} q_2 n_2 \mu_2^2}{(q_1 n_1 \mu_1 + q_2 n_2 \mu_2)^2}. \tag{35}$$

If the mobilities and concentrations of electrons and holes in the semiconductor structure are equal, their charges completely compensate each other when in magnetic field, and the Hall effect does not occur. If there is no such symmetry in the concentration and the mobility an uncompensated Hall potential is generated. As a result a transverse Hall field arises which retards the movement of electrons towards the negatively charged surface

and at the same time accelerates holes towards it. The process of charge accumulation continues until the hole and electron currents balance each other. Thus the Hall voltage is reduced. Moreover, a carrier concentration gradient arises and transverse diffusion currents flow in the sample. Nonuniform carrier distribution causes temperature gradients and results in an additional hall voltage offset.

The most important figure of merit of any type of sensor is the sensibility S. This parameter is determined as the ratio of the variation in the output signal to the variation in the external measured value at constant other parameters. The absolute voltage and current sensitivities of the hall sensor are defined (15)

$$S_A^{(V)} = \left|\frac{\partial V}{\partial B}\right|_c, \quad [VT^{-1}], \tag{36}$$

$$S_A^{(I)} = \left|\frac{\partial I}{\partial B}\right|_c, \quad [AT^{-1}]. \tag{37}$$

The constancy of all other parameters is denoted by the index *c*. The relative magnetosensitivity is determined by the ratio of the absolute sensitivity to the supply current or the voltage applied. The current-related sensitivity is defined when the input is fed by current I_s

$$S_{RI}^{(V)} = \frac{S_A^{(V)}}{I_s}\left|\frac{1}{I_s}\frac{\partial V}{\partial B}\right|_c, \quad [VA^{-1}T^{-1}], \tag{38}$$

$$S_{RI}^{(I)} = \frac{S_A^{(I)}}{I_s}\left|\frac{1}{I_s}\frac{\partial V}{\partial B}\right|_c, \quad [T^{-1}]. \tag{39}$$

For the voltage-related sensitivity similar expressions are defined

$$S_{RV}^{(V)} = \frac{S_A^{(V)}}{V_s}\left|\frac{1}{V_s}\frac{\partial V}{\partial B}\right|_c, \quad [T^{-1}], \tag{40}$$

$$S_{RV}^{(I)} = \frac{S_A^{(I)}}{V_s}\left|\frac{1}{V_s}\frac{\partial V}{\partial B}\right|_c, \quad [AV^{-1}T^{-1}]. \tag{41}$$

V_s denotes the applied voltage.

CHAPTER 2

THE HALL EFFECT SENSOR

2.1. Structure of the Hall Sensor

In classical Hall sensors it is impossible to obtain both a high sensitivity and a low thermal drift. The sensitivity of devices made of narrow band gap materials is highly dependent upon temperature. Materials with a large band gap have a rather low mobility, that also limits sensitivity. The use of a III-V 2DEG system is an effective method of achieving simultaneously a high electron mobility and a low sheet carrier density, which is essential to obtain a high sensitivity of magnetic field sensor.

In conventional semiconductor devices only one type of semiconductor is used throughout. If more than one semiconductor material is used, causing a change in the energy bands within the structure, this type of devices is termed a hetorostructure (25). The ability to tailor the energy-band structure adds flexibility to the design of devices based on doping and materials variations in the various layers. The changes in the energy band provide an additional means, independent of doping, to control the distribution of charge carriers throughout these devices.

When two semiconductor materials with different bandgaps are joined together to form a heterojunction, discontinuities in both the conduction- and a valence-band edges occur at the heterointerface (23). The conduction and valence-band offsets at the heterointerface are calculated from an electron affinity rule.

2 DEG in the $In_{0.75}Ga_{0.52}As/In_{0.52}Al_{0.48}As$ heterostructure is formed in InGaAs layer due to the conduction band offset. Electrons from donors located in InAlAs layers are trapped in the quantum well formed by the energy offset.

2.2. 2DEG System

A cross-section of the sensor structure is shown in Fig. 2.1. Approximately 1μ of undoped $In_{0.52}Al_{0.48}As$ is grown by MBE on a semi-insulating InAs substrate, followed by about 50A channel of $In_{0.75}Ga_{0.25}As$. The channel is covered by $In_{0.52}Al_{0.48}As$ layer of which the first part thickness d_s is undoped and forms a spacer, the upper part of the layer is doped with Si at a level of about $n \sim 10^{18}$ cm^{-3}.

The growth of the $In_{0.52}Al_{0.48}As$ buffer on the substrate is necessary to get good-quality interface. This compound is lattice matched to InP. The $In_{0.75}Ga_{0.25}As$ channel acts as a quantum well for electrons because of the energy offset. The channel represents an active layer, which contains the high mobility electron gas. The spacer increases the spatial separation between electrons and donors located in the $In_{0.52}Al_{0.48}As$ barrier layer which is doped with Si.

The $In_{0.53}Ga_{0.47}As$ cap layer is doped and serves to make good ohmic contacts. The cap is removed from the active area after forming contacts.

Schematic band diagram of the structure shows that a potential well formed between the buffer layer and the barrier (Fig. 2.2).

Electrons supplied by donors of the barrier are trapped into the well and remain confined in the channel. The concentration of carriers is therefore significantly varies throughout

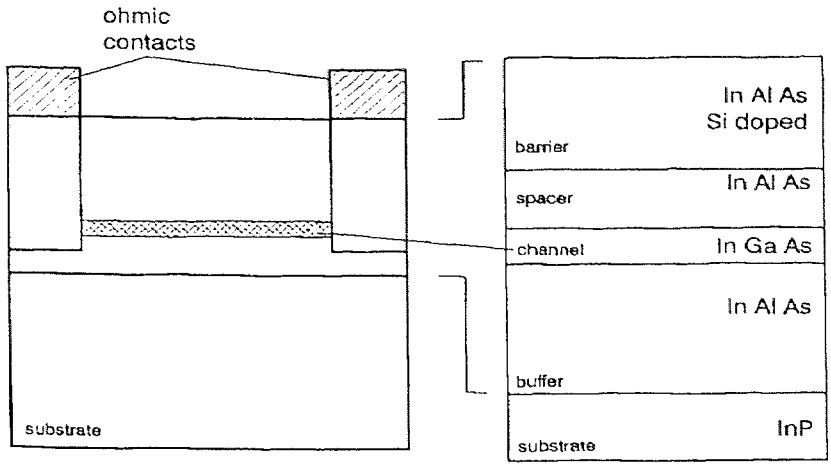

Fig. 2.1. Schematic diagram of the physical structure of the hall effect sensor.

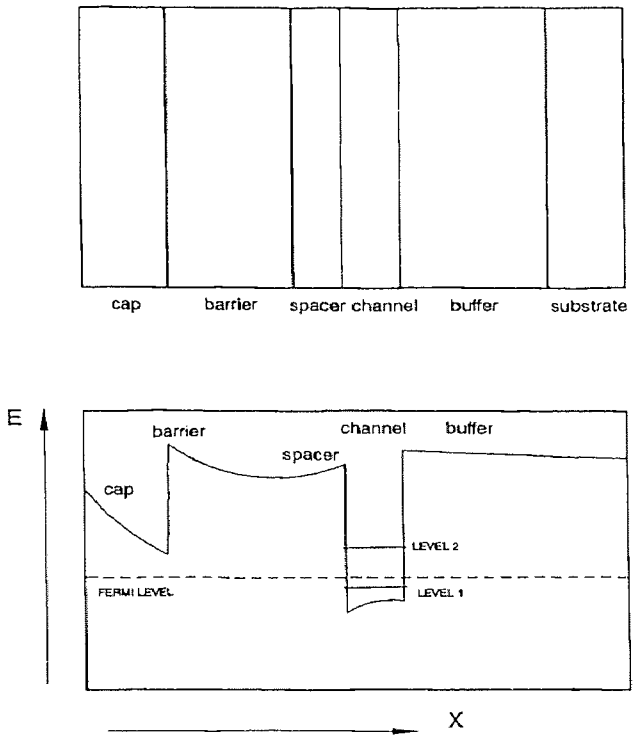

Fig. 2.2. Schematic band diagram of the InGaAs/InAlAs hall sensor.

the structure. That implies that only the channel is regarded as a conductive layer.

Because the width of the confining potential is comparable with the electron wavelength, quantum effects are important. A set of discrete energy levels is defined for electron motion in the direction perpendicular to the surface. However, electrons are free to move in the plane of the $In_{0.75}Ga_{0.25}As$ channel and behave therefore as a two-dimensional degenerate electron gas.

The role of the spacer layer is to separate electrons confined in the channel from the ionized donor atoms. If the ionized donors are located at the distance from the drifting electrons there is no scattering on the donor centers. Thus ionized impurity scattering is very much reduced, as compared with bulk $In_{0.75}Ga_{0.25}As$ (30).

2.3. The Sheet Carrier Density in the Channel

The concentration of carriers in the channel is defined as two-dimensional concentration (sheet carrier density) since only a thin layer contains the electron gas and the concentration of electrons around the layer is comparatively low. The motion of electrons in the plane is free and the electron eigenstates are the plane waves (12). The electron motion perpendicular to the interface is quantized and all the charges reside in the lowest bound state of the quantum well (10) (Fig. 2.3).

The density of plane wave states is a constant in two dimensions and depends only on the effective mass of electron m*:

$$D_0 = \frac{m^*}{\pi\hbar^2},$$

including spin degeneracy.

For $In_{0.75}Ga_{0.25}As$, with effective mass $m^*/m \sim 0.045$, the density of electron states is about $2 \cdot 10^{10}$ $meV^{-1}cm^{-2}$. The occupancy of the states is determined by position of the Fermi level. The ground electron level is located at 60 meV below the Fermi level and thus fully occupied (Fig. 2.2) . The first excited state of the confining potential is about 0.1 eV above the Fermi level and is nearly empty. Therefore the sheet carrier density is roughly 10^{12} carriers per cm^2 (4,8).

In sandwich structures the sheet carrier density may be controlled by the parameters of the structure. Hence the properties of the system are flexible depending on the fabrication conditions.

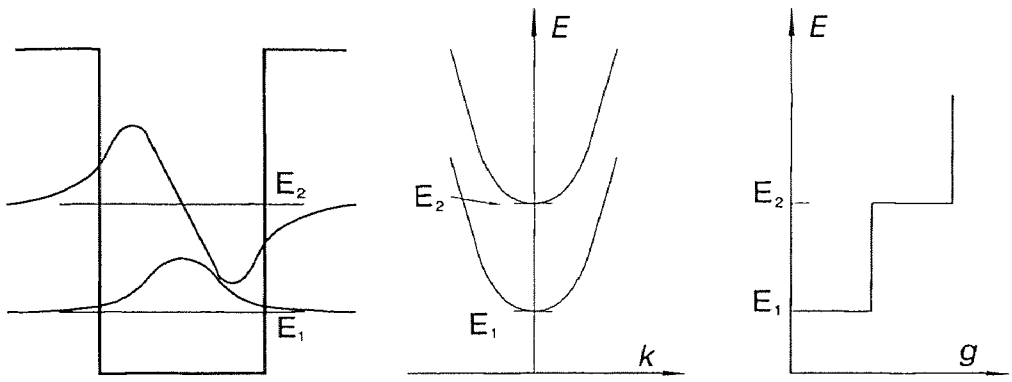

Fig. 2.3. The main properties of the rectangular quantum well: the energy diagram, the dispersion relationship, and the density of states diagram.

.There are several factors that influence the sheet carrier density: doping level of the barrier, spacer thickness, and channel thickness.

The energy levels of bound electrons in the channel depend on both the barrier height and the quantum well width. Relative positions of the channel conduction band and that of the barrier layer determine the quantum well depth and may be varied by material composition changes. The width of the well corresponds to the channel thickness and thus may be varied for optimization of the sensor performance. MBE technology provides possibilities to grow a film as thin as 20A. The theoretical sheet carrier density as the channel thickness function for $In_{0.75}Ga_{0.25}As/In_{0.52}Al_{0.48}As$ hall sensor with the barrier thickness 400A is plotted in Fig. 2.4 (4).

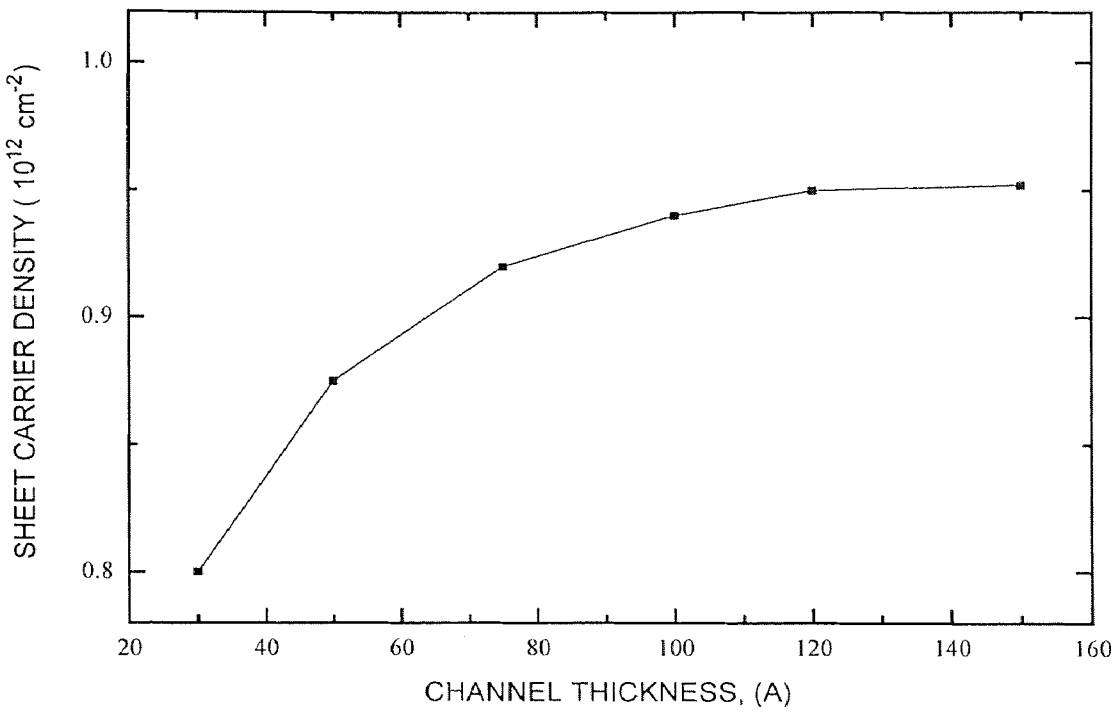

Fig 2.4. Sheet carrier density as the function of the channel thickness (data from Ref. (4)).

For a thickness less than 70A the total charge carrier density in the channel decreases because of confinement effects: confinement energy increases and the number of states decreases. The sheet carrier density was found to be almost independent of the In/Ga mole fraction ratio (15).

Modulation of the sheet carrier density is also possible by varying the doping concentration of the barrier. The sheet carrier density decreases with the doping level (3,4).

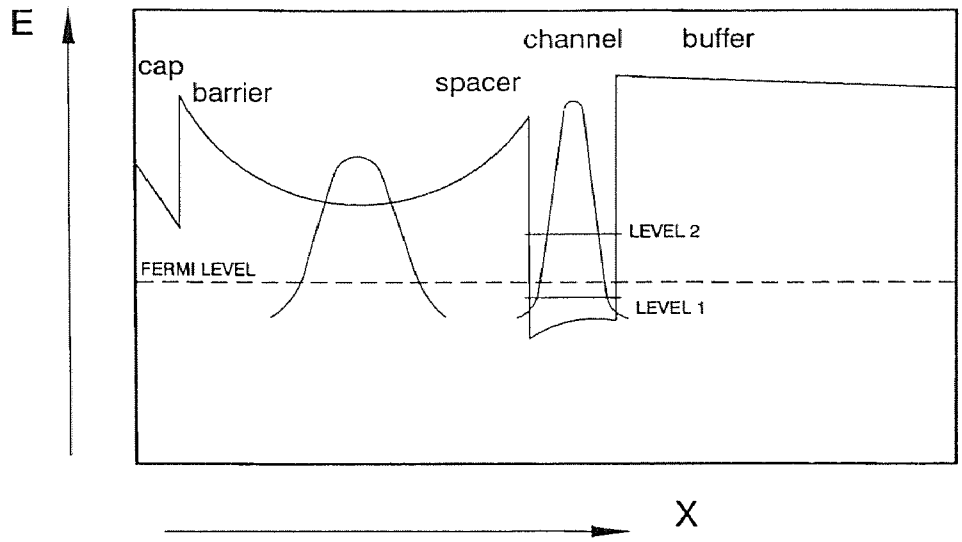

Fig. 2.5. Parallel conduction in the barrier.

An important requirement for the system is to maintain only a thin layer of active carriers. Across the structure the concentration of carriers must be negligible comparatively to that in the channel. The $In_{0.75}Ga_{0.25}As/In_{0.52}Al_{0.48}As$ structure provides a depletion in the

barrier and a high resistance of the buffer. An additional conductive channel may be formed in the barrier if its width is sufficient. Then there are two conduction paths: the 2DEG of the channel and the nondepleted zone in the barrier. The structure with parallel conduction in the barrier is shown in Fig. 2.5.

The factor responsible for the parasite conduction is the width of the barrier. The dependence of the channel carrier density on the doping level is affected by the width of the spacer, the nondoped region of the barrier.

2.4. Electron Mobility in the Channel

In general carriers in a semiconductor are scattered by their interaction with the following excitations (16): acoustic phonons, optical phonons (for polar crystals), ionized impurities, neutral defects, interfaces, other carriers. For room temperatures the phonon scattering mechanism is dominant in most semiconductors. Particularly in polar semiconductors optical phonon interaction with electrons is stronger than other mechanisms. Mobility of electrons is determined by scattering. Studies of the hall mobility in InGaAs 2DEG manifest that for room temperature the dominant mechanism is optical phonon scattering (5). It implies that the spacer thickness is not critical for achieving a high mobility. Similar systems with the spacer thickness of 20A and 60A had the same mobility at 300K. Ionized impurity scattering influence the electron mobility only at low temperature.

The electron mobility increases with increasing In mole fraction of $In_xGa_{1-x}As$ (3). The highest electron mobility at room temperature in the $In_{0.52}Al_{0.48}As/In_xGa_{1-x}As$ heterostructure was obtained for x=0.8.

2.5. Temperature Dependence

In general the mobility of carriers decreases with temperature. The effect is significant at low temperatures. At room temperatures mobility continue decreasing but at much lower rate. The temperature dependence of the Hall mobility and the sheet carrier density in the InGaAs 2DEG at room temperatures is summarized in the Fig.2.6 (3).

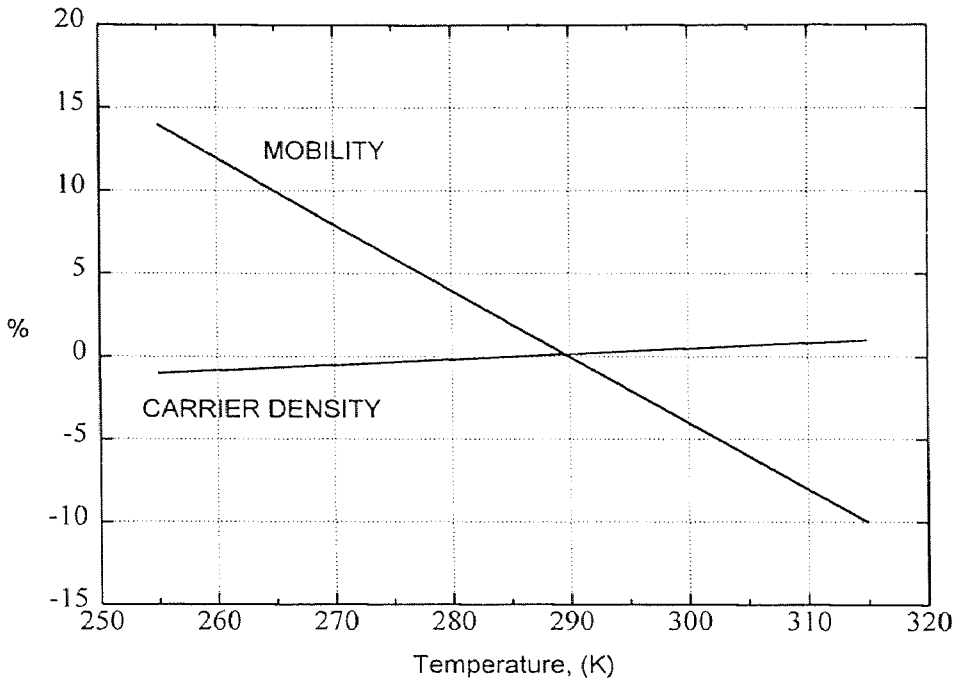

Fig 2.6. Temperature dependence of the electron mobility and the sheet carrier density (data from Ref. (3)).

Several factors influence the thermal behavior of the electron density in a 2DEG system. First, the distance of the Fermi level E_F from the bottom of the conduction band is temperature dependent. Thus, the equilibrium free electron density in the channel varies in order to maintain the electrostatic equilibrium of the structure. However, because of the small effective mass of the electrons (m^*/m~0.045 in $In_{0.75}Ga_{0.25}As$), the sheet electron density is very small and the channel is degenerate even for small (~10^{12} cm^{-1}) carrier density. Thus the temperature dependence of the sheet carrier density is week.

A second factor is the temperature dependence of the hall scattering factor r_H. However, because of the degeneracy of the conduction band the hall factor remains practically equal to unity in the range of room temperatures.

A parasitic parallel conduction in the potential well formed by the band curvature in the confining barrier layer is responsible for another temperature effect. A high doping density in the large bandgap barrier layer ensures a sharp curvature of the conduction band in the confining layer and thus contribute to the parallel conduction being negligible.

Finally, as long as the doping impurities are not fully ionized, their ionization factor depends on the temperature.

In summary the $In_{1-x}Ga_xAs/In_{0.52}Al_{0.48}As/InP$ heterostructure provides a possibility to vary In-Ga ratio in the compound and subsequently change the properties of the structure.

The $In_{0.75}Ga_{0.25}As/In_{0.52}Al_{0.48}As/InP$ heterostructure was considered. Aspects of energy band structure were analyzed. This approach seems to be the most informative for

modeling of the sensor. All the important parameters can be deduced from the band structure of the device. Temperature influence upon the device performance is also reflected in the energy band structure.

High electron mobility and low carrier concentration in the channel of the device result in excellent sensitivity of the device. These parameters in the $In_{0.75}Ga_{0.25}As/In_{0.52}Al_{0.48}As/InP$ heterostructure showed a weak temperature dependence at room temperatures.

CHAPTER 3

DISCUSSIONS

3.1 The Hall Sensor Materials

In chapter 1 a low concentration of charge carriers and high carrier mobility were mentioned to be preferred properties of materials for hall element fabrication. Semiconductors are the materials that meet these requirements. The concentration of electrons in metals is about 10^{22} cm^{-3}, that is higher by several orders of magnitude than that in semiconductors. The hall coefficient in Au or Cu, for instance, is $R_H \sim 10$ cm^3C^{-1} (18) whereas in Si the hall coefficient is $R_H \sim 10^5$ cm^3C^{-1}(18, 24). Insulators usually manifest very low mobility.

According to the Eq. (32) the intensity of the hall effect is proportional to the hall coefficient R_H, the only parameter reflecting properties of the material. The hall coefficient is inversely proportional to the carrier concentration, that makes a semiconductor with the low concentration of doping impurities suitable for achieving the high performance of the sensor.

The hall voltage V_H is proportional to the carrier mobility according to the Eq. (31). Therefore the sensor material used should have high carrier mobility μ.

The two parameters are the primary criteria for the choice of a semiconductor material but not the only ones.

The bandgap width E_g must be taken into consideration as well. The carrier concentration and mobility in semiconductor materials are temperature dependent. Thus the semiconductor hall sensor performance is affected by temperature conditions. This negative influence is strong in narrow-bandgap semiconductors.

Materials parameters of selected semiconductors important for galvanomagnetic sensors at 300K are listed in table 1.

Table 1. Electron structure parameters of selected semiconductors.

Material	electron mobility $\mu_n,(m^2V^{-1}s^{-1})$	hole mobility $\mu_n,(m^2V^{-1}s^{-1})$	Bandgap $E_g,(eV)$
Ge	0.39	0.19	0.67
Si	0.14	0.05	1.12
GaAs	0.85	0.045	1.42
InAs	2.5	0.046	0.36
InSb	7.5	0.075	0.17

Despite the major advantage of semiconductors, the principal drawback which is the existance of the two types of carriers, holes and electrons, limits the performance of semiconductor hall sensors. From the expression (31) for the hall voltage it follows that it depends on the sign of charge carriers. The hall voltage V_H has a positive value in case

it is generated by deflection of holes and a negative value if it is generated by electrons. The hall voltage measured is the sum of those produced by electrons V_n and holes V_p

$$V=V_n+V_p.$$

Most of the semiconductors manifest electron mobility much higher than that of holes. For that reason n-type semiconductors are most often used in hall devices.

3.2. Band Structures of InGaAs and InAlAs Alloys

The ideal semiconductor for the Hall sensor fabrication should have one type of charge carrier with a high mobility at room temperatures. Its properties should also be weakly influenced by temperature and applied electric field. These material characteristics are derived from the energy band structure.

The mobility is defined as the ratio of carrier velocity to applied field. The velocity is inversely proportional to an effective mass m^*, which is determined by the k-space curvature of relevant bandedge. Unfortunately, electron mobility for semiconductors varies inversely with minimum band gap, which restricts achievment of a high mobility and a low temperature drift of properties simultaneously.

An influence of the applied electric field appears because scattering rates are dependent on the energy of a scattered electron. In general, as carrier energies increase, new scattering mechanisms come in effect and the mobility decreases. Phonon scattering usually dominates at room temperature (31, 33). The efficiency of this mechanism varies in semiconductors due to energy band structure and it is significant if several energy minima in conduction band provide a large variety of scattering paths.

Table 2 contains a collection of the band gap information of III-V compounds at 300K that are used in 2DEG systems.

Table 2. Energy band gaps and effective masses of alloys used in the structure

Compound	Energy Band Gap (eV)	Conduction Band Edge Effective Mass Ratio to the Free Electron Mass
GaAs	1.424	0.066
AlAs	2.153	0.19
InAs	0.354	0.024
InP	1.344	0.077

The energy band gap for a semiconductor alloy $A_xB_{1-x}C$ is a variation of energy gap of fundamental compounds AC and BC. Energy bands of $In_xGa_{1-x}As$, as functions of the fraction ratio x are often approximated by a quadratic form (29). There lowest conduction band gaps are plotted in the Fig. 3.1.

The direct Γ gap is the minimum gap throughout the whole alloy concentration. The energy gap decreases with increasing of InAs constituent. The calculated energy gap for the composition $In_{0.75}Ga_{0.25}As$ calculations is equal E_g=0.

The energy gap of the confining layers is larger than that of the channel. Results of the similar calculations for the band gap in $In_xAl_{1-x}As$ plotted in the Fig. 3.2.

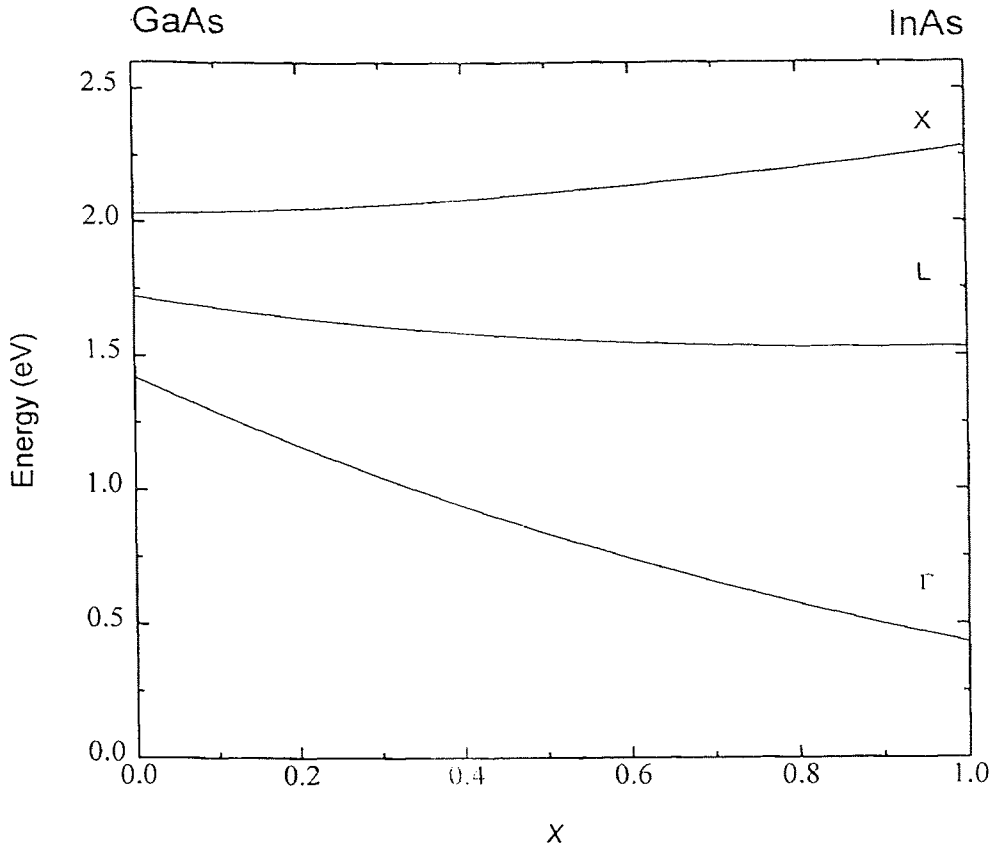

Fig. 3.1. Conduction band energy minimum at Γ, *X*, and *L* relative to the top of the valence band as functions of alloy composition *x* in $In_xGa_{1-x}As$.

The minimum gap for x=1 (InAs) is a direct gap of 0.42 eV at Γ. This continues to be the minimum gap as x decreases until the Γ gap crosses the X gap at a crossover concentration x=0.276, and with a gap E_g=2.1 eV. For x<0.276 the X gap is the smallest among the three gaps. The composition $In_{0.52}Al_{0.48}As$ lattice-matchs InP substrate. The concentration ratio corresponds to the energy gap of 1.45 eV.

Another important structure parameter that depends on composition of alloys is the lattice parameter. It is of the first consideration when designing heterostructure. To grow a structure of a good quality, lattice parameters of adjacent layers should be very close.

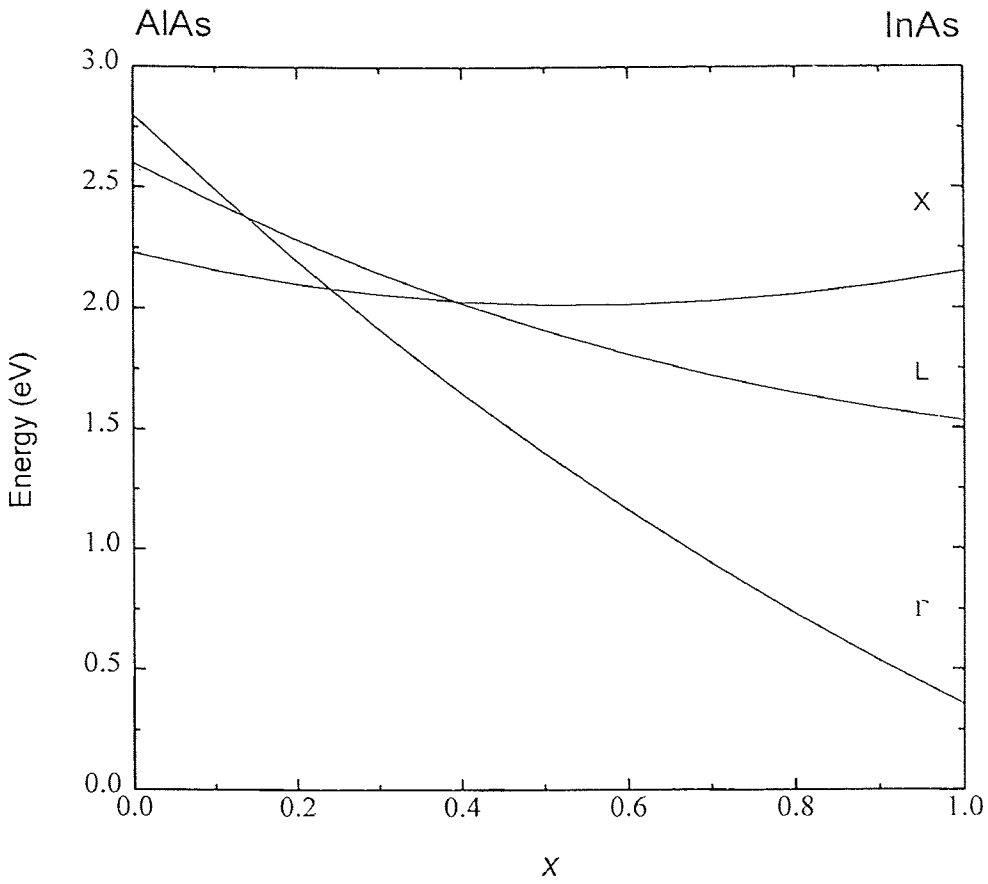

Fig. 3.2. Conduction band energy minimum at Γ, *X*, and *L* relative to the top of the valence band as functions of alloy composition *x* in $In_xAl_{1-x}As$

The lattice alignment is known as pseudomorphic growth. The lattice parameter of a compound $A_{1-x}B_xC$ can be approximated by a linear interpolation between the values of the constituents AC and BC. Semiconductor alloys used in the proposed hall sensor, GaAs, AlAs, and InAs , form the zincblende crystal structure and have lattice parameters 5.65 A, 5.62 A, and 6.04 A respectively. The lattice constant of InP used as a substrate has a value of 5.86 A. Linear interpolation gives the lattice parameter of 5.84 A for the

compound $In_{0.52}Al_{0.48}As$. That fact implies that the buffer layer of $In_{0.52}Al_{0.48}As$ perfectly matches InP substrate.

Having identical lattice constant is not a necessary condition for pseudomorphic growth of one semiconductor on another. It is possible to force the epitaxial layer to have the same lattice constant as the substrate even though they may be different in the bulk. The crystal structure of such an epilayer is strained because it must match the crystal structures of confining layers at the boundaries. However there is a limit to the thickness of a strained layer one can growth while maintaining a perfect epilayer. As the strain energy increases with the thickness, beyond some thickness mechanical stresses in the layer can relieve the strain via creating of misfit dislocations. Strained pseudomorphic layers of $In_{1-x}Ga_xAs$ exhibit properties that differ from those observed in the bulk compound. The electron mobility in a channel of a pseudomorphic $In_{1-x}Ga_xAs$ layer at the heterointerface of $In_{0.52}Al_{0.48}As$ undoped layer decreases with Ga mole fraction x. The highest electron mobility of 16000 $cm^2\ V^{-1}s^{-1}$ at room temperatures corresponds to the value of x=0.2. The lattice-matched $In_{0.53}Ga_{0.47}As$ layer manifests a mobility 20% lower. The lattice parameter of $In_{0.75}Ga_{0.25}As$ according to the linear interpolation a= 5.94 A. A thickness of the channel layer in the $In_{0.75}Ga_{0.25}As/In_{0.52}Ga_{0.48}As$ structure should be less than critical, which is about 150 A.

3.3. Device Geometry

In chapter 1 the hall effect theory was applied in the limits of the infinitely long and the infinitely short hall element. Neither of the conditions is completely fulfilled in most real hall sensors. The behavior of the devices is somewhere between that of very long and very short samples.

The effect of the geometry upon the hall voltage in a sample of arbitrary shape in described by introducing a geometrical correction factor G (17, 38)

$$G = \frac{V_H}{V_{H\infty}}. \tag{42}$$

$V_{H\infty}$ denotes the hall voltage that correspond to the infinitely long sample and defined by the expression (31). The voltage V_H is a characteristic of the actual device. The numerical value of the factor G varies within the interval $0 \le G \le 1$ and approaches unity in the limit of the very long sample. The factor G depends not only the length-width ratio but on the contact size and the hall angle. A decrease in the Hall voltage V_H is attributed to the imperfect spatial confinement of the current in the sample. In general the factor G is a function of the length-to-width ratio, Hall contact size s, and the Hall angle θ_H:

$$G = f(\frac{L}{W}, \frac{s}{W}, \theta_H). \tag{43}$$

In order to increase the efficiency of Hall sensors the analysis can be conducted with respect to the classical rectangular shape sample. The dependence of the Hall voltage on ratio L/W and θ_H can be approximated by the expression:

$$G = 1 - \frac{16}{\pi^2}\exp(-\frac{\pi L}{2W}) \cdot \left[1 - \frac{8}{9}\exp(-\pi\frac{L}{W})\right] \cdot (1 - \frac{\theta_H^2}{3}), \tag{44}$$

for the length-to-width ratio: $0.85< L/W<\infty$; and the Hall angle θ_H: $0<\theta_H<0.45$ (17, 35). The geometrical factor G approaches unity when ratio $L/W=4$ and can be eliminated in the considerations. As the distance between the low-resistance supply contacts and Hall terminals is increased, a possibility of the Hall voltage shunting by the contacts diminishes. The sample may be regarded as a long plate with good accuracy. The consideration of a Hall terminal size results in a correction to the G-factor. For contacts as small as 1/20 of W, the effect is negligible.

3.4. Operation of the Hall Sensor

3.4.1. The Hall Voltage

The Hall voltage can be measured in two modes: forcing of a constant current through the Hall element, or application of a constant voltage to the sensor contacts. Hall sensors are often supplied by a constant voltage V. In this mode of operation the hall voltage V_H is bounded to the voltage V by means of the expression (31)

$$V_H = -\mu_H \frac{W}{L} B V_x . \tag{45}$$

It follows from the expression that at constant applied voltage the hall voltage increases with an increase in the ratio W/L. For a very short sample the geometrical factor is determined from the expression (44). The maximum value of the hall voltage V_H with a fixed product VB results from the combination of the equations (44) and (45)

$$V_H \cong 0.742 \mu_H VB. \tag{46}$$

The hall voltage when operating the sensor in the constant voltage mode is linearly proportional to the Hall mobility. The constant current mode of operation provides independence of the Hall voltage of the mobility. The expression (32) implies that the carrier concentration and the thickness of the channel are the parameters that affect the Hall voltage. It is inversely proportional to the product of the density and thickness.

2 DEG Hall sensors reported in literature showed good linearity against magnetic field in the range ±0.3 T.

3.4.2. The Offset Voltage

The offset voltage is a dc signal, induced by imperfections of the sample. Many factors contribute to the offset:

i) Geometrical misalignment of the hall voltage terminal with respect to the equipotential plane in the sensor.

ii) Crystal damage due to the fabrication process as a result of which regions of local resistivity variations appear in the active sensor layer;

iii) Nonuniform temperature distribution in the hall element. The temperature gradient across the sensor results in a resistivity imbalance and an additional offset. The temperature difference introduce a thermoelectric potential between the hall terminals. Nonuniformity in temperature can be a result of the variation in sheet resistivity across the structure due to uneven thickness of the channel.

The offset voltage due to misalignment of the sensor contacts can be calculated

$$V_{\text{off}} = \frac{I}{q\mu_{\text{H}} nWt}\Delta l, \tag{47}$$

where Δl is the geometrical misalignment of the sensor contacts with respect to the equipotential plane and t denotes a thickness of the active channel.

3.4.3. Signal-to-Noise Ratio

In a constant magnetic field the offset voltage can not be distinguished from the useful signal. Signal-to-noise (SNR) ratio can be introduced as the ratio of the Hall and the offset voltage. The expressions for these values can be used to obtain SNR

$$\text{SNR} = \mu_{\text{H}} B \frac{W}{\Delta l}. \tag{48}$$

3.4.4. Sensitivity

The supply current magnetic sensitivity is defined combining the expression for relative magnetosensitivity and the expression for the Hall voltage

$$S_I = G\frac{r_{\text{H}}}{qnt}. \tag{49}$$

The supply voltage-related sensitivity is defined similarly

$$S_V = G\frac{W\mu_{\text{H}}}{L}. \tag{50}$$

The voltage related sensitivity increases as the effective length of the structure decreases, yet there is an upper physical limit .

3.5. Conclusions

The Hall effect sensor using 2DEG in the $In_{0.75}Ga_{0.25}As/In_{0.52}Al_{0.48}As/InP$ heterostructure was discussed. Parameters and estimated characteristics of the device are listed in the table 3.

Table 3. Parameters and estimated characteristcis of the $In_{0.75}Ga_{0.25}As/In_{0.52}Al_{0.48}As/InP$ 2DEG Hall device.

Size, $L \times W$	0.25×0.2 mm^2
Active Layer	$In_{0.75}Ga_{0.25}As$ 2DEG
Active Layer Thickness	20 A
Spacing Thickness	50 A
Barrier Thickness	4000 A
Barrier Doping Concentration	10^{18} cm^{-3}
Electron Mobility	14000 cm^2 V^{-1} s^{-1}
Sheet Carrier Density	0.8×10^{12} cm^{-2}
Absolute Sensitivity	3.2 V T^{-1}

Energy band structure of the system showed to have the most important influence on the performance of the sensor.

Effects of composition of $In_{1-x}Ga_xAs$ and $In_{1-y}Al_yAs$ compounds such as the energy gap dependence and the effective mass dependence were considered. The structure of the real

sensor can be optimized in order to meet a certain requirements of applications. This fact makes the discussed sensor potentially useful in variety of applications.

Capabilities of the sensor are defined by properties of materials of which the sensor is made, geometry of the device, and operating conditions. Electrical parameters of the hall sensor were discussed. The hall voltage, a signal directly corresponding to the magnetic field, is linearly proportional to the magnetic field induction.

Device characteristics such as electron mobility and sheet carrier density determine the response of the sensor to the magnetic field. The offset voltage, a signal that limits a minimal magnetic field to be measured depends on the geometry of the device and can be optimized. Magnetic sensitivity integrates the geometry and material characteristic impact. An operation mode must be chosen to achieve the best performance of the device. Most important merit of the $In_{0.75}Ga_{0.25}As/In_{0.52}Al_{0.48}As/InP$ hall sensor is that provides high sensitivity at room temperatures, the condition that limit the performance of SQUID devices. The sensor with discussed structure may also exhibit a good performance at lower temperatures. The electron mobility and the charge carrier density, parameters that proved to be the most important for the Hall sensor, even take advantage of the low temperature conditions. However temperature sensitivity of these characteristics is increasing and very stable conditions are required at low temperatures. Substantial freedom in the structure design make possible various optimization when modeling a sensor for another operating conditions.

REFERENCES

1. S. Del Medico, T. Benyattou, G. Guillot, M. Gendry, T. Venet, J. Tardy, A. Chovet, *Proceedings of the 3rd ICIM/ECSSM*, **289-293**, 1996

2. S. Del Medico, T. Benyattou, G. Guillot, M. Gendry, M. Oustric, T. Venet, J. Tardy, G. Hollinger, A. Chovet, N. Mathieu, *Sensors and Actuators, A*, 46-47, **298-301**, 1996

3. Y. Sugiyama, T. Taguchi, M. Tacano, *Sensors and Actuators, A*, 34, **131-136**, 1992

4. S. Del Medico, T. Benyattou, G. Guillot, M. Gendry, M. Oustric, T. Venet, J. Tardy, G. Hollinger, A. Chovet, N. Mathieu, *Semiconductor Science and Technology*, v 11, 4, **576-581**, 1996

5. V. Mosser, S. Contreras, S. Aboulhouda, Ph. Lorenzini, F. Kobbi, J. L. Robbert, K. Zekentes, *Sensors and Actuators, A*, 43, **135-140**, 1996

6. Y. Sugiyama, T. Taguchi, M. Tacano, *Proceedings of the 6th Sensor Symposium*, **55-60**, 1986
7. Y. Sugiyama, H. Soga, M. Tacano, *Journal of Crystal Growth*, 95, **394-397**, 1989.

8. J. Eisenstain, *Proceedings of a NATO ASI on Interfaces, Quantum Wells, and Superlattices, NATO ASI series, B*, v. 179, **271-298**, 1987

9. F. Koch, *Proceedings of a NATO ASI on Interfaces, Quantum Wells, and Superlattices, NATO ASI series, B*, v. 179, **67-94**, 1987

10. G. Bastard, *Proceedings of a NATO ASI on Interfaces, Quantum Wells, and Superlattices, NATO ASI series, B*, v. 179, **189-210**, 1987

11. H. Baltes, R. Castagnetti, *Semiconductor Sensors*, **205-269**, John Wiley & Sons, New York, 1994

12. N. Ashcroft, N. Mermin, *Solid State Physics*, Holt, Rinehart and Winston, New York, 1976

13. V. Bonch-Bruevich, S. Kalashnikov, *Physics of Semiconductors*, Nauka, Moscow, 1979

14. S. Pearton, N. Shah, *High-Speed Semiconductor Devices*, **283-310**, John Wiley & Sons, New York, 1994

15. Y. Sugiyama, *Sensors and Materials*, 5, 6, **317-328**, 1994

REFERENCES
(Continued)

16. C. Ridley, *Quantum Processes in Semiconductors*, Clarendon, Oxford, 1988

17. C. Roumenin, *Solid State Magnetic Sensors*, Elsevier Science B. V., Amsterdam, 1994

18. N. Mathieu, A. Chovet, M. Chertouk, *Sensors and Materials*, 5, 6, **359-368**, 1994

19. Y. Sugiyama, *Journal of Vacuum Science & Technology, B*, 13, 3, **1075-1083**, 1995

20. R. Kyburz, J. Schmid, R. Popovic, H. Melchior, *IEEE Transactions on Electron Devices*, 41, 3, **315-320**, 1994

21. H. Blanchard, L. Chiesi, R. Racz, R. Popovic, *Proceedings of the 1996 IEEE International Electron Devices Meeting*, **541-544**, 1996

22. N. Mathieu, A. Chovet, R. Fauquembergue, P. Descherdeer, A. Leroy, Sensors and Actuators, A, 27, 1-3, **741-745**, 1991

23. Yu and M. Cardona, *Fundamentals of Semiconductors: Physics and Materials Properties*, Springer-Verlag Berlin Heidelberg,1996

24. R. Popovic, *Sensors and Actuators, A*, 17, 1-2, **39-53**, 1989

25. J. Bean, *High-Speed Semiconductor Devices*, **13-38**, John Wiley & Sons, New York, 1994

26. N. Kuze, I. Shubasaki, *III-V review*, 10, 1, **28-32**, 1997

27. S. in't Hout, S. Middelhoek, *Sensors and Actuators, A*, 37-38, **26-32**, 1993

28. Z. Stoessel, M. Resch, *Sensors and Actuators, A*, 37-38, **449-452**, 1993

29. A. Chen, A. Sher, *Semiconductor Alloys, Physics and Materials Engineering*, Plenum Press, New York, 1995

30. M. Herman, H. Sitter, *Molecular Beam Epitaxy: Fundamentals and Current Status*, Springer-Verlag Berlin Heidelberg, 1989

31. P. Blood, J. Orton, *The Electrical Characterization Of Semiconductors: Majority Carriers and Electron States*, Academic Press, San Diego, 1992

REFERENCES
(Continued)

32. R. Prange, S. Girvin, *The Quantum Hall Effect*, Springer-Verlag Berlin Heidelberg,1990

33. P. Butcher, N. March, M. Tosi, *Physics of Low-Dimensional Semiconductor Structures*, Plenum Press, New York, 1993.

34. B. Hu, E. Souza, W. Knox, J. Cunningham, M. Nuss, A. Kuznetsov, S. Chuang, *Physics Rewiew Letters*, 74, 9,**1689-1692**, 1995

35. J. Heremans, *Journal of Physics, D*, 26, **1149-1168**, 1993